JACS
JOURNAL OF THE AMERICAN CHEMICAL SOCIETY

ARTICLE

pubs.acs.org/JACS

Theoretical Prediction on the Thermal Stability of Cyclic Ozone and Strong Oxygen Tunneling

Jien-Lian Chen and Wei-Ping Hu*

Department of Chemistry and Biochemistry, National Chung Cheng University, Chia-Yi, 621, Taiwan

Supporting Information

ABSTRACT: Dual-level dynamics calculation with variational transition state theory including multidimensional tunneling has been performed on the isomerization reaction of cyclic ozone → normal (open) ozone, which was believed to be the stability-determining reaction of the elusive cyclic ozone molecule under thermal condition. The high-level potential energy surface data were obtained from the calculation using the MRCISD+Q theory with the aug-cc-pVQZ basis set, while the low-level reaction path information was obtained using the hybrid density functional theory B3LYP with the cc-pVTZ basis set. The calculated results showed very significant tunneling effects below 300 K (a factor of ~200 at 300 K and over 10^7 at 200 K). Because of the strong tunneling effects and the potential energy surface crossing of the $1A_1$ and $1A_2$ states, the isomerization reactions were found to be significantly faster than previously believed. The half-life of the cyclic ozone was estimated only ~10 s at 200 K and ~70 s below 100 K, which might partly explain the unsuccessful attempts for its experimental identification. The kinetic isotope effects (KIEs) for various ^{18}O substitution reactions were also calculated as a function of temperature and were as high as 10 at very low temperature. Because of the large KIEs, the experimental identification of the cyclic $^{18}O_3$ seems more promising.

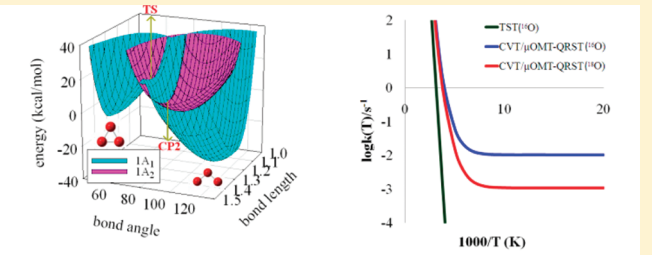

Calculated PES and Arrhenius Plot for cyclic O_3 → open O_3

INTRODUCTION

Ozone is a fascinating molecule in many ways. A thin layer of ozone in the stratosphere absorbs a significant amount of ultraviolet light from the sun, and thus forms a protective shield for life in the troposphere and on the surface of the earth. The depletion of the ozone layer, which was discovered 40 years ago, catalyzed by man-made chemicals such as chlorofluorocarbons (CFCs) and halons, has been of great environmental concern and has attracted numerous experimental and theoretical studies.[1−15] On the other hand, the formation of ozone near the surface caused by air pollution in the cities is hazardous to the health of city residents.[16] In addition to its wide industrial applications, ozone was also used in chemical synthesis.[6,17] In quantum chemistry, despite its small size, ozone is a notoriously difficult molecule to study due to the multireference properties of its electronic structure.[18] A less well-known mystery of ozone is that it might have an isomer with the structure of an equilateral triangle (D_{3h} point group), "cyclic ozone" (see Figure 1). The cyclic form of ozone satisfies the stable lewis structure (perfect octet for all three oxygen) without using the concept of resonance. From high-level theoretical study,[19−24] it is now established that cyclic ozone is approximately 30 kcal/mol higher in energy than the "normal" (or "open") form of ozone. However, theory also predicted a significant energy barrier of ~24 kcal/mol for the isomerization from the cyclic form to the open form. The energy of cyclic ozone was also calculated to be 6−7 kcal/mol higher than that of ground-state dioxygen and oxygen atom, and the energy barrier for this dissociation channel was predicted to be as high as 47 kcal/mol.[19] Thus, the intrinsic thermal stability of cyclic ozone is determined by the isomerization reaction. (This also implies that starting from O_2 + O to produce cyclic ozone, the reaction is endoergic and the system has to overcome a very high barrier. The reaction would probably end up mostly with the open form of ozone, which is 26 kcal/mol lower in energy than O_2 + O. Even if a small amount of the cyclic O_3 can be produced from O_2 + O, its stability is still determined by the isomerization reaction.) From a theoretical point of view, the cyclic ozone should be a kinetically stable molecule and should show up in suitable experimental conditions. However, to our knowledge, no firm experimental evidence on the existence of cyclic ozone has been obtained despite an extensive search in the last two decades. Explanations have been proposed for the unsuccessful attempts.[19,24,25] In particular, the topology of the O_3 potential energy surface (PES) may cause the regions in the vicinity of cyclic ozone to be inaccessible under the experimental conditions either from the open form of ozone or from O + O_2 in the ground electronic states.[19,22,24] Another possible explanation is that the isomerization reaction from the cyclic form to the open form is fast, and the lifetime of the cyclic ozone is too short to be identified spectroscopically. Although the barrier for the isomerization is as high as 24 kcal/mol, the reaction involves relatively

Received: April 28, 2011
Published: September 02, 2011

dx.doi.org/10.1021/ja203428x | J. Am. Chem. Soc. 2011, 133, 16045–16053

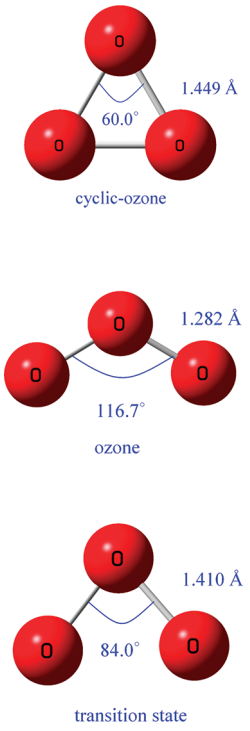

Figure 1. Calculated structures of the ozone, from top: cyclic ozone, open ozone, and the transition state.

small nuclear motions of the oxygen atoms. As a result, the width of the energy barrier is short, and thus the dynamics contribution from the tunneling effects cannot be ignored. In the current study, we applied the variational transition state theory including multuidimensional tunneling (VTST/MT)[26−29] corrections to calculate the unimolecular rate constants of the isomerization reaction as a function of temperature. The results would give a good estimate on the importance of the tunneling effects and thus the lifetime of the elusive cyclic ozone to the correct order of magnitude. These data would thus be essential in a future experimental search for the cyclic ozone molecule.

METHOD

The dual-level[30] VTST/MT method was used in the current study to calculate the thermal rate constants. The method requires a qualitatively correct "low-level" potential energy surface (PES), which is calculated on the fly as required during the VTST/MT calculation. We selected the unrestricted B3LYP density functional theory[31,32] with the cc-pVTZ basis set[33] (UB3LYP/cc-pVTZ) to calculate the low-level PES. The low-level reaction path was calculated from −1.9 to 3.2 bohrs with a gradient step size of 0.01 bohr and a Hessian step size of 0.05 bohr using the Page−McIver method[34,35] in the mass-scaled coordinates with a scaling mass of 1 amu. The selection of the low-level theory was based on the calculated molecular geometry and reaction energetics in comparison to the high-level multireference calculation done previously and in the current study. Although the ozone system under study is well-known to be a multireference system, we found that the UB3LYP/cc-pVTZ method performed relatively well as compared to other traditional wave function-based single-reference methods, such as MP2.[36] Although using the complete active space (CAS or CASSCF)[37]method is also an option for calculating the low-level PES, we found that the CASSCF calculation did not give reliable energy gradients in the transition state region, and thus made the force constant (Hessians) calculation rather cumbersome. The coupled-cluster calculations at UCCSD(T)[38] level with aug-cc-pVTZ and aug-cc-pVQZ[33] basis sets were also performed on the open and cyclic ozone and on the isomerization transition state for comparison. The dual-level VTST also requires a set of "high-level" geometry and energy data on the stationary points along the reaction path for the interpolated corrections to the low-level PES. The high-level geometries were obtained at the MRCISD+Q[39,40]/aug-cc-pVTZ level, and the energies data were obtained using a larger basis set at the MRCISD+Q/aug-cc-pVQZ level, both with a full-valence active space (18 electrons in 12 orbitals). The wave function was optimized using a state-averaged (SA) approach including the three lowest electronic states ($1A_1$, $2A_1$, $1A_2$ in C_{2v} classification). The SIL-1 interpolated correction scheme[41] was applied in the dual-level calculation using the MRCISD+Q/aug-cc-pVTZ energies along the low-level reaction path geometry to estimate the barrier width. Thermal rate constants as a function of temperature were calculated at the conventional transition state theory (TST) and the canonical variational theory (CVT)[26] levels. The microcanonical optimized multidimensional tunneling (μOMT)[27] correction was evaluated at continuous energy levels (the conventional method) and at quantized reactant states (the QRST method)[42,43] along the reaction path. The bending mode (in C_{2v} classification, because the geometry on the reaction path is in C_{2v} symmetry) of the cyclic ozone was selected to approximate the reaction-path mode on the reactant side of the reaction path, and the harmonic approximation was used to determine the quantized reactant-state energy levels in the QRST calculation. The electronic structure calculation was performed using the Gaussian 03[44] and Molpro[45] programs, and the dual-level VTST/MT calculation was performed using the Gaussrate 8.2[46] program, which is an interface between the Gaussian 03 and Polyrate 8.2 programs.[47]

RESULTS AND DISCUSSION

a. Molecular Geometry. Figure 1 shows the calculated geometry of open ozone, cyclic ozone, and the transition state (TS) of the isomerization reaction between these two conformations. Table 1 lists the geometrical parameters obtained at various theoretical levels and available experimental data.[48] Most of the data obtained from the literature were also recalculated and confirmed in the current study. For ozone, the calculated ground-state structures were all in good agreement with experiments. For cyclic ozone, all calculations predicted a D_{3h} structure with three equal O−O bond lengths of ∼1.45 Å. The multiconfigurational calculation of the TS geometry of the isomerization reaction was known to be a difficult case for convergence[19,24] and was constrained to the C_{2v} point group. The calculated TS geometries by the unrestricted coupled-cluster, MP2, and B3LYP methods were all in the C_{2v} point group. At the MRCISD+Q level, the two equivalent O−O bond lengths of the TS were predicted to be 1.410 Å, and the predicted bond angle was 84°. This indicates an "early" TS for the cyclic ozone → ozone isomerization because the TS geometry is similar to that of the cyclic ozone. It has been known that the $2A_1$ electronic state has a conical intersection with the $1A_1$ state at the vicinity of the TS of the $1A_1$ state.[19,24] This intersection is not expected to have significant effects on the thermal reaction at low temperature because, as will be mentioned later in this Article, tunneling at energies well below that of the TS totally dominates the isomerization reaction. It has also been known that the $1A_2$ state crosses the $1A_1$ state both on the cyclic ozone and on the open ozone sides.[19] The dynamical implication of the crossings between the $1A_1$ and $1A_2$ states, however, has not been carefully studied before. We found that the crossings actually intersect with the reaction path on the $1A_1$ surface. As a result, thermal reactions following the adiabatic path

Table 1. Calculated Bond Lengths (in angstroms) and Bond Angles (in degrees)

	open ozone		cyclic ozone		transition state		CP1		CP2	
	R(O−O)	A(O−O−O)	R(O−O)	A(O−O−O)	R(O−O)	A(O−O−O)	R(O−O)	A(O−O−O)	R(O−O)	A(O−O−O)
UB3LYP/cc-pVTZ	1.256	118.2	1.432	60.0	1.381	77.9				
UMP2/aug-cc-pVTZ	1.284	116.7	1.457	60.0	1.366	82.0				
UCCSD(T)/aug-cc-pVTZ	1.277	117.0	1.447	60.0	1.395	79.2				
CASSCF(18,12)/aug-cc-pVTZ	1.291	116.7	1.457	60.0	1.427	83.8	1.416	80.3	1.406	89.2
MRCISD+Q(18,12)/aug-cc-pVTZ	1.282	116.7	1.449	60.0	1.410	84.0	1.416	79.7	1.401	89.6
MCSCF(18,12)/ANO-L3 ζ[a]					1.430	83.6				
MS-CASPT2(18,12)/ANO-L3 ζ[a]	1.281	117.0	1.449	60.0						
MCSCF(FORS)/cc-pVTZ[b]	1.292	116.5	1.466	60.0	1.426	83.9				
MCSCF(18,12)/aug-cc-pVQZ[c]	1.283	117.0	1.448	60.0						
MCSCF(12,9)/cc-pVQZ[d]	1.275	116.5	1.442	60.0	1.430	83.6				
exp[e]	1.273	116.8								

[a] From ref 24. [b] From ref 20. [c] From ref 23. [d] From ref 22. [e] From ref 48.

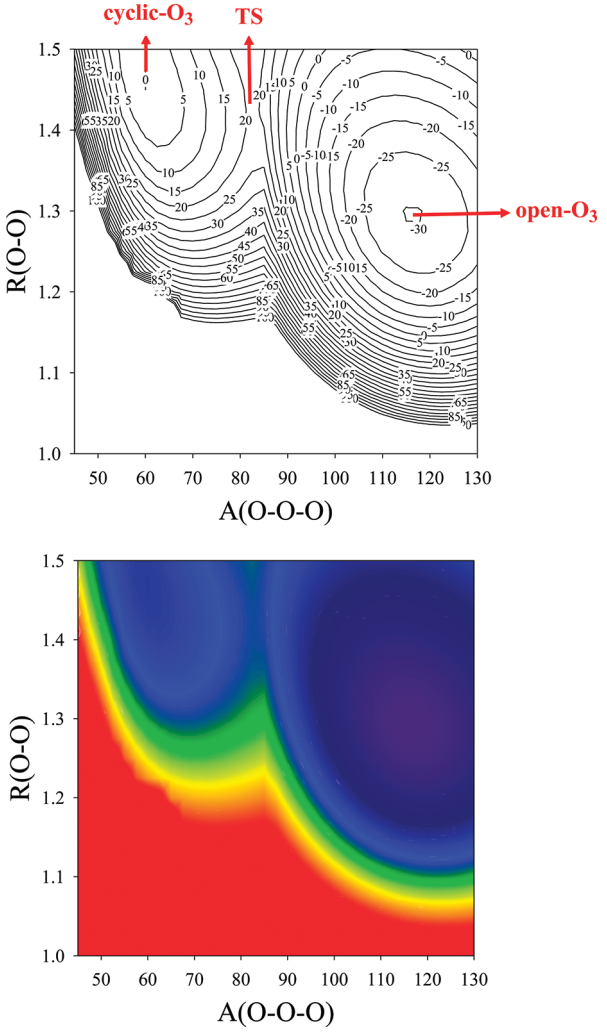

Figure 2. The $1A_1$ potential energy surface of ozone calculated at CASSCF/aug-cc-pVTZ level (bond distance in angstroms and bond angles in degrees).

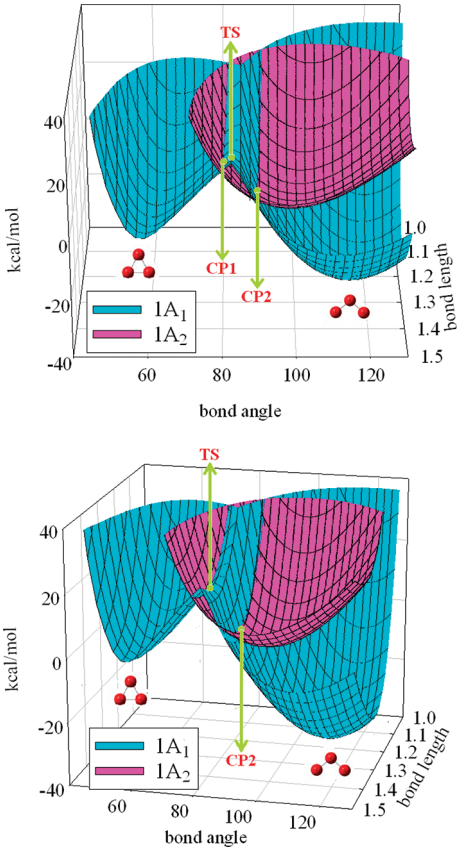

Figure 3. Calculated $1A_1$ and $1A_2$ potential energy surfaces at C_{2v} geometry from two perspectives (top view and side view). The bond lengths are in angstroms and bond angles are in degrees.

would experience a lower effective barrier than the $1A_1$ PES suggests. This will be discussed in more detail in the next sections. Figure 2 shows a two-dimensional plot of the $1A_1$ PES, and Figure 3 shows the three-dimensional PES including both $1A_1$ and $1A_2$ states using the CASSCF/aug-cc-pVTZ theory at C_{2v} symmetry. The cyclic and open ozone can be clearly seen as energy minima on the left- and right-hand sides, respectively. The two conformations are separated by a high and long "ridge" as seen in the middle of the figures. The $1A_1$ transition state is located at the "opening" of the ridge. As seen in Figure 3, the

dx.doi.org/10.1021/ja203428x |J. Am. Chem. Soc. 2011, 133, 16045–16053

Table 2. Calculated Relative Energies (kcal/mol)

	cyclic ozone	open ozone	transition state	CP1	CP2
UB3LYP/cc-pVTZ	0.0	−28.6	17.1		
UMP2/aug-cc-pVTZ	0.0	−36.7	24.1		
UCCSD(T)/aug-cc-pVTZ	0.0	−29.0	19.3		
UCCSD(T)/aug-cc-pVQZ[a]	0.0	−29.5	19.8		
CASSCF(18,12)/aug-cc-pVTZ	0.0	−30.2	23.0	19.0	6.9
MRCISD+Q/aug-cc-pVTZ	0.0	−30.7	25.1	19.9	7.1
MRCISD+Q/aug-cc-pVQZ[b]	0.0	−31.5	25.8	21.1	8.1
MS-CASPT2(18,12)/ANO-L3 ζ[c]	0.0	−33.5	22.2		
MCSCF(FORS)/cc-pVTZ[d]	0.0	−30.0	22.8		
MRCISD/aug-cc-pVQZ//MCSCF(18,12)/aug-cc-pVQZ[e]	0.0	−31.4			
MRCISD+Q/cc-pVQZ//MCSCF(12,9)/cc-pVQZ[f]	0.0	−31.1	23.9		

[a] Using UCCSD(T)/aug-cc-pVTZ structures. [b] Using MRCISD+Q/aug-cc-pVTZ structures. [c] From ref 24. [d] From ref 20. [e] From ref 23. [f] From ref 22.

crossings of the $1A_1$ and $1A_2$ states occur on either sides of the central ridge and intersect with the $1A_1$ reaction path at CP1 and CP2. The structures of these two points were located by first finding the reaction path geometry on the $1A_1$ PES predicted by CASSCF/aug-cc-pVTZ calculation, and then searching for the structures that were on the path with degenerate $1A_1$ and $1A_2$ (CASSCF or MRCISD+Q) energies. The calculated structures of CP1 and CP2 are shown in Table 1. At the CASSCF level, the calculated O−O bond length and the O−O−O bond angle of CP1 were 0.01 Å shorter and ∼4° smaller than those in $1A_1$ TS, while the corresponding values of CP2 were 0.02 Å shorter and ∼5° larger. At the vicinity of the $1A_1$ TS, the reaction path depends primarily on the bond angle.

b. Reaction Energetics. Table 2 shows the calculated reaction energetics. All of the calculations with high-level electron correlation, in particular, the coupled-cluster and multireference configuration interaction theory, predicted that the cyclic ozone is 29−34 kcal/mol higher in energy than the open ozone. The isomerization barrier was predicted to be 22−25 kcal/mol relative to the cyclic ozone by the MCSCF and MRCI methods, while the CCSD(T) and the B3LYP methods predicted a lower barrier of 17−20 kcal/mol. Because the ozone is a well-known multireference system, the former value is believed to be more reliable. To our knowledge, the highest theoretical level for energy calculation reported on the isomerization reaction is the MRCISD+Q/cc-pVQZ calculation by Schinke and Bittererova.[23] We further augmented the basis set with diffuse functions (the aug-cc-pVQZ basis set) in the current study, and the calculated energy of reaction and barrier height on the $1A_1$ surface were −31.5 and 25.8 kcal/mol, respectively. The energies of CP1 and CP2 relative to the cyclic ozone were predicted to be 21.1 and 8.1 kcal/mol, respectively, at the MRCISD+Q/aug-cc-pVQZ level. Thus, to a good approximation, the effective thermal barrier is lowered by 4.7 kcal/mol due to the $1A_1-1A_2$ crossing. The energy of reaction (−31.5 kcal/mol) and the adiabatic barrier height (21.1 kcal/mol) calculated at the MRCISD+Q/aug-cc-pVQZ level were used in the current study as the high-level energy data in the dual-level VTST/MT calculation. The unrestricted B3LYP, MP2, and UCCSD(T) calculations were carried out without symmetry constraints on the wave function, and the lowest-energy state was calculated. Thus, the TS obtained can be regarded as an approximation to the crossing point CP1, and the barrier heights are calculated as an approximation to the adiabatic barrier. The calculated B3LYP/cc-pVTZ reaction path, which served as the low-level PES data in the current study, can thus be regarded as an approximation to the adiabatic reaction path. The calculated dual-level energy profiles along the reaction path are shown in Figure 4.

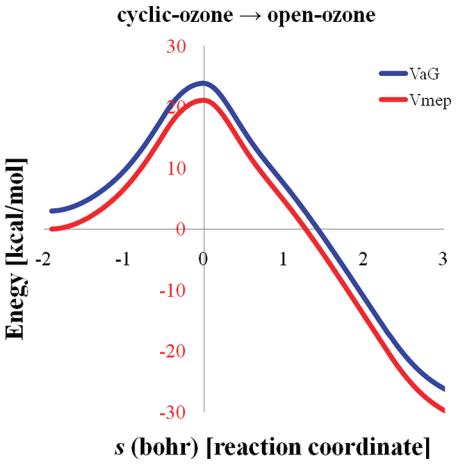

Figure 4. The calculated dual-level energy profiles along the reaction path. The V_{mep} is the relative classical (Born−Oppenheimer) energy, and the V^a_G is V_{MEP} plus the vibrational zero-point energy.

c. Rate Constants and Tunneling. Table 3 lists the calculated dual-level rate constants from 25 to 500 K, and the corresponding Arrhenius plot is shown in Figure 5. The TST rate constants were found to span 165 orders of magnitude in this temperature range because of the relatively high barrier height (21.1 kcal/mol). As shown in the table, at the same temperature, the calculated CVT rate constants were very similar to the TST rate constants, which indicates the variational effects in the current system are negligible. This is in fact expected because the TS structure is similar to that of the reactant (cyclic-O_3), and the vibrational zero-point energies do not change significantly along the reaction path. Thus, the reaction bottleneck is dominated by the large classical (or Born−Oppenheimer) barrier. Inclusion of the tunneling corrections made the temperature dependence of the rate constants much less dramatic at low temperature. This corresponds to the well-known "curvature" in the Arrhenius plot (Figure 5). Tunneling effects are usually very pronounced in reactions involving hydrogen (or proton) transfer if there is a significant energy barrier.[26,27,49−51] Recently, significant tunneling effects

Table 3. Calculated Rate Constants (s^{-1}) and Half-life (s)

T(K)	TST	CVT	CVT/ μOMT	CVT/ μOMT-QRST	half-life[b]
25	3.83(−161)[a]	3.61(−161)	2.46(−4)	1.03(−2)	6.74(+1)
50	1.63(−74)	1.58(−74)	6.03(−4)	1.03(−2)	6.70(+1)
75	1.46(−45)	1.43(−45)	1.15(−3)	1.04(−2)	6.69(+1)
100	4.74(−31)	4.67(−31)	2.07(−3)	1.04(−2)	6.66(+1)
125	2.55(−22)	2.52(−22)	3.82(−3)	1.09(−2)	6.33(+1)
150	1.74(−16)	1.72(−16)	7.73(−3)	1.36(−2)	5.10(+1)
175	2.62(−12)	2.59(−12)	1.83(−2)	2.34(−2)	2.97(+1)
200	3.62(−9)	3.59(−9)	5.28(−2)	5.87(−2)	1.18(+1)
250	9.34(−5)	9.29(−5)	7.39(−1)	7.77(−1)	8.92(−1)
300	8.40(−2)	8.36(−2)	1.41(1)	1.46(1)	4.73(−2)
400	4.33(2)	4.31(2)	3.60(3)	3.90(3)	1.78(−4)
500	7.53(4)	7.50(4)	2.43(5)	2.82(5)	2.45(−6)

[a] 3.83(−161) means 3.83×10^{-161}. [b] Based on the CVT/μOMT-QRST rate constants.

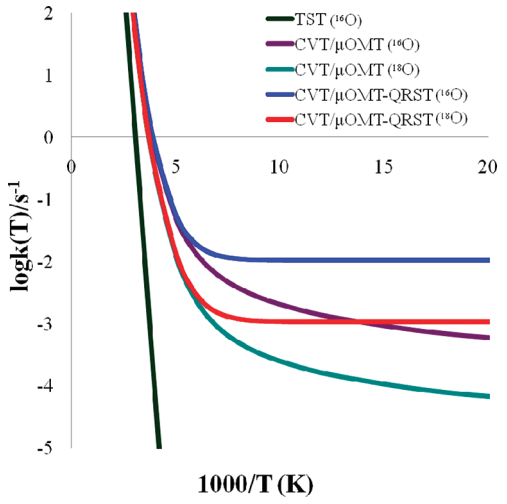

Figure 5. The Arrhenius plot of the calculated rate constants for the cyclic ozone → open ozone reaction. The curves for $^{16}O^{16}O^{16}O$ are labeled (^{16}O), and the curves for $^{18}O^{18}O^{18}O$ are labeled (^{18}O). The TST (^{18}O) curve would almost overlap with the TST (^{16}O) curve completely in this Arrhenius plot and is thus not shown.

corresponding to the movement of carbon atoms have been reported.[52,53] To our knowledge, however, large tunneling effects have not been reported corresponding specifically to the movement of oxygen atoms in chemical reactions. In the current system, the overall structural changes are small while the energy barrier is high, and this translates into a narrow barrier width and high tunneling probabilities. As seen in Table 3, the predicted rate constant by the CVT/μOMT method was approximately 3 times the value by the TST method at 500 K. This indicated the tunneling and the over-the-barrier processes are almost equally important around this temperature. Below 500 K, the tunneling is the major contribution to the reaction rates. For example, the calculated CVT/μOMT rate constants were ~200, 10^7, and 10^{27} times higher than the TST values at 300, 200, and 100 K, respectively. The calculated rate constants using continuous and discrete tunneling energies were similar above 200 K. However, as shown in Figure 5, the QRST rate constants leveled

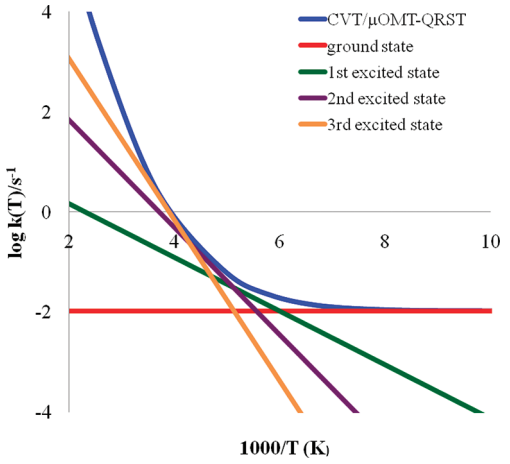

Figure 6. Arrhenius plot and the tunneling contribution from the first four reactant states to the CVT/μOMT-QRST rate constants.

off below 150 K and reached the asymptotic value of ~1×10^{-2} s^{-1} while the rate constants calculated by the conventional tunneling method continued to decrease as the temperature decreased. This is because below 150 K essentially all of the reactant molecules are at the vibrational ground state, and in the QRST calculation the relative population among the quantized states and thus the overall tunneling contribution do not change appreciably as the temperature further decreases. Figure 6 showed the tunneling contributions from the first few quantized reactant states (of the reaction-path vibrational mode) as a function of temperature. As seen in the figure, above 250 K, the tunneling from higher vibrational excited states dominated the tunneling rate constants. However, the contributions from these excited states decreased very rapidly as the temperature decreased. At ~200 K, the first excited state became the dominant one, and below ~150 K, all the tunneling contribution came almost exclusively from the vibrational ground state. Similar trends have been reported in previous QRST studies.[42,43,51b] On the other hand, in the conventional tunneling method, which is based on the continuous tunneling energies, the relative population at various energy states is still a sensitive function of the temperature. At 50 K, the predicted rate constant by the QRST method was approximately 17 times higher than that by the conventional tunneling methods. The asymptotic value of the CVT/μOMT-QRST rate constant translates to a half-life of 67 s. Thus, our current study predicts that the cyclic ozone is not a kinetically very stable molecule even at low temperature. At 200 and 300 K, the predicted half-lives were 12 and 0.05 s, respectively. This could partly explain the so far unsuccessful attempts in the experimental identification of the cyclic ozone molecule.

d. Kinetic Isotope Effects. Five types of ^{18}O isotope substitutions are possible, and they are $^{18}O^{16}O^{16}O$, $^{16}O^{18}O^{16}O$, $^{18}O^{18}O^{16}O$, $^{18}O^{16}O^{18}O$, and $^{18}O^{18}O^{18}O$. The first and the second substitutions result in identical reactants (cyclic ozone) but different products, and thus correspond to different reaction paths. Similarly, the third and the fourth substitutions result in the same reactants but different reaction paths. Table 4 showed the calculated CVT/μOMT-QRST rate constants for all of the isotope substitutions. It is noted that different symmetry numbers (as specified below the table) were used for some of the substitutions due to the different rotational symmetry numbers of the reactants and transition states. While there are five types

Table 4. Calculated Rate Constants[a] (s^{-1}) by CVT/μOMT-QRST

T(K)	$^{16}O^{16}O^{16}O$	$^{16}O^{18}O^{16}O$	$^{18}O^{16}O^{16}O$	$^{18}O^{16}O^{18}O$	$^{18}O^{18}O^{16}O$	$^{18}O^{18}O^{18}O$
25	1.03(−2)[b]	1.34(−3)	1.91(−3)	5.82(−4)	1.42(−3)	1.06(−3)
50	1.03(−2)	1.34(−3)	1.91(−3)	5.83(−4)	1.42(−3)	1.06(−3)
75	1.04(−2)	1.35(−3)	1.92(−3)	5.83(−4)	1.42(−3)	1.07(−3)
100	1.04(−2)	1.35(−3)	1.93(−3)	5.88(−4)	1.44(−3)	1.08(−3)
125	1.09(−2)	1.43(−3)	2.04(−3)	6.39(−4)	1.55(−3)	1.19(−3)
150	1.36(−2)	1.81(−3)	2.62(−3)	8.85(−4)	2.10(−3)	1.75(−3)
175	2.34(−2)	3.20(−3)	4.76(−3)	1.86(−3)	4.21(−3)	4.08(−3)
200	5.87(−2)	8.27(−3)	1.26(−2)	5.84(−3)	1.26(−2)	1.44(−2)
250	7.77(−1)	1.20(−1)	1.92(−1)	1.12(−1)	2.27(−1)	3.31(−1)
300	1.46(1)	2.67(0)	4.50(0)	2.74(0)	5.43(0)	8.77(0)
400	3.90(3)	9.77(2)	1.80(3)	9.69(2)	1.93(3)	2.97(3)
500	2.82(5)	7.89(4)	1.51(5)	7.39(4)	1.48(5)	2.13(5)

[a] Symmetry numbers used in $^{16}O^{16}O^{16}O$, $^{18}O^{16}O^{16}O$, $^{16}O^{18}O^{16}O$, $^{18}O^{18}O^{16}O$, $^{18}O^{16}O^{18}O$, and $^{18}O^{18}O^{18}O$ reactions were 3, 2, 1, 2, 1, and 3, respectively. [b] 1.03(−2) means 1.03×10^{-2}.

Table 5. Calculated KIEs by TST and CVT/μOMT-QRST

	KIE1		KIE2		KIE3	
T(K)	TST	CVT/μOMT-QRST	TST	CVT/μOMT-QRST	TST	CVT/μOMT-QRST
25	1.64	3.16	2.79	5.14	4.86	9.68
50	1.29	3.17	1.68	5.15	2.20	9.71
75	1.19	3.18	1.41	5.16	1.69	9.72
100	1.14	3.18	1.30	5.15	1.48	9.67
125	1.11	3.15	1.23	5.00	1.37	9.19
150	1.09	3.07	1.19	4.55	1.30	7.75
175	1.08	2.94	1.16	3.85	1.25	5.73
200	1.07	2.81	1.14	3.18	1.22	4.07
250	1.05	2.50	1.11	2.29	1.17	2.35
300	1.04	2.04	1.09	1.79	1.14	1.67
400	1.04	1.40	1.07	1.34	1.11	1.31
500	1.03	1.23	1.06	1.27	1.10	1.33

of ^{18}O substitutions, there are only three types of experimentally observable rate constants due to the single, double, and triple substitutions. Thus, in the KIEs calculation, the rate constants for the two single-substitution reactions were summed up as a single rate constant $k(^{18}O\text{-}1)$. Similarly, the rate constants calculated for the two double-substitution reactions were summed up as a single rate constant $k(^{18}O\text{-}2)$. The rate constants of the unsubstituted and triply substituted reaction are designated as $k(^{16}O)$ and $k(^{18}O\text{-}3)$, respectively. We define three types of KIEs as follows:

$$\text{KIE1} = k(^{16}O)/k(^{18}O\text{-}1) \quad (1)$$

$$\text{KIE2} = k(^{16}O)/k(^{18}O\text{-}2) \quad (2)$$

$$\text{KIE3} = k(^{16}O)/k(^{18}O\text{-}3) \quad (3)$$

The calculated KIEs using the TST and CVT/μOMT-QRST theory are shown in Table 5 and Figure 7. The three types of KIEs were found to be significant at low temperature when tunneling effects were considered. The KIE1, KIE2, and KIE3 by CVT/μOMT-QRST theory approached asymptotic values of 3, 5, and 10, respectively, below ~150 K. This is somewhat surprising because the mass difference of the isotopes is relatively small and the oxygen atom is quite heavy. From Table 5 and Figure 6, it is obvious that the tunneling effects increased the KIEs significantly below 250 K before the KIEs reached the asymptotic values below ~150 K. The increase was due to the higher tunneling contributions to the $k(^{16}O)$ than to the various isotope substituted rate constants. Thus, although the mass difference between ^{16}O and ^{18}O is small, the very short barrier width makes the tunneling effects still sensitive to the isotope substitutions. The predicted large KIEs mean the substituted cyclic ozone has longer lifetime and may be easier to identify experimentally. The future observation of the large KIEs would be a strong evidence of oxygen tunneling.

e. Connections to Experiments and Other Ring-Opening Reactions. While cyclic ozone has long been known to be a minimum-energy structure on the potential energy surface with significant barriers for isomerization and unimolecular dissociation, its lifetime was unknown, and thus it has been difficult to design suitable experiments to identify its existence. The current results indicate that the isomerization rate constants and thus its lifetime are sensitive functions of temperature above 200 K. For example, at room temperature, the lifetime was predicted to be only 0.05 s and much shorter at higher temperature. Thus, the

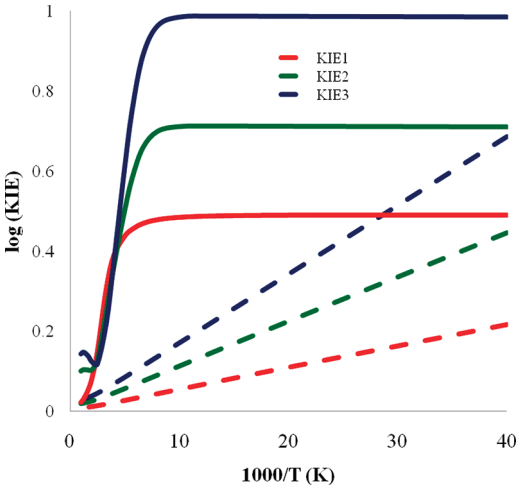

Figure 7. Temperature dependence of the calculated KIEs. The broken and solid lines indicate results calculated at TST and CVT/μOMT-QRST levels, respectively.

calculation suggested that very effective cooling techniques, for example, matrix isolation or cryogenic solvent,[54−57] must be employed during the experimental generation and detection of cyclic ozone molecules. It is especially crucial if the cyclic ozone is generated from singlet oxygen atom and singlet dioxygen because they are significantly higher in energy than cyclic ozone. The lifetime of cyclic ozone is predicted to be ∼10 s at 200 K, ∼50 s at 150 K, and reaches the asymptotic value of ∼70 s below 100 K. Because of the properties of the ground-state tunneling, further lowering of temperature would not increase the lifetime. Thus, cooling significant below 100 K in experiment was not absolutely necessary. While the predicted lifetime at low temperature is certainly within the reach of the current experimental techniques, the experimentalists need to be aware that the data accumulation time is rather limited even after effective cooling. For example, if one wishes to use FT-IR to identify the cyclic ozone in a matrix, the effective data accumulation time is only ∼1 min. Higher concentration of cyclic ozone might need to be generated to obtain the fingerprint absorption with good S/N ratios. With a lifetime on the order of 10 s, laser spectroscopy, in principle, is applicable to identify the cyclic ozone if the excited-state information is available. The experimentalists could use the published excited-state data[19,20,24] and those included in the Supporting Information from the current study to design suitable spectroscopic study. One should also be aware that if one wishes to generate cyclic ozone by laser photolysis of O_3 or O_2 in a matrix, the same laser beam may also dissociate the newly generated cyclic O_3.

The current research also implies that in other ring-opening reactions, if the movements of the atoms (or equivalently, the barrier widths) are small and the reactions have sizable energy barriers, the tunneling effects might dominate the reactions at lower temperature even though the atoms in the ring are relatively heavy such as carbon, nitrogen, or oxygen. For example, one might expect that the ring-opening reaction of cyclopropane, which is isoelectronic to cyclic ozone, to propylene also has significant tunneling effects. Earlier studies showed that this reaction is exoergic with a high energy barrier,[58−60] and the distance between the two terminal carbon atoms increases by ∼1.0 Å[59] during the reaction. In comparison, the distance between the two terminal oxygen atoms in the current system increases by only ∼0.7 Å. More importantly, the TS of the current system is "early" with a bond angle of ∼84° and a terminal O−O distance larger than the cyclic form by only 0.4 Å, while the corresponding TS of the cyclopropane is very "late" with a bond angle of ∼128° and a terminal C−C distance larger than the cyclic form by 1.1 Å. This effectively makes the barrier width of the ring-opening reaction of cyclopropane much larger than that of the current system. In fact, the tunneling effects were not apparent from the available experimental rate constants of this reaction.[61] The same argument on the structure comparison between the cyclic form and the TS can also be made to the ring-opening of oxirane,[62,63] dioxyirane,[64,65] and cyclic N_3[56,66,67] systems, which have been studied previously. Because of the relatively "late" TS, those systems are not expected to have tunneling effects as significant as in the current system. The experimental decomposition rate constants of oxirane[62] at 350−440 °C did not show signs of strong tunneling effects. Furthermore, if the energy of the ring-opening product is higher in energy than the cyclic form, for example, as calculated in the case of dioxirane,[64,65] the ground-state tunneling channel would not be open. Instead of leveling off at a temperature much higher than the absolute zero, the rate constant would continue to decrease as the temperature decreases even if the reaction is dominated by tunneling. It is also very interesting to compare the current results with the recent work by Borden, Singleton, and co-workers on the ring-opening reaction of cyclopropylcarbinyl radical.[52c,d] They showed that significant carbon tunneling occurred below 150 K. The predicted TS structure was very "early" with the opening C−C−C bond angle increased from 61° in the reactant to 80° in the TS, and the distance of the C−C bond that was being broken increased only 0.4 Å from the cyclic form to the TS. These structure differences are surprisingly similar to those predicted in the current study. Because of the relatively low barrier heights (8.4 kcal/mol), the tunneling effects and the KIEs in the ring-opening reaction of cyclopropylcarbinyl radical were less dramatic than those predicted in the current study.

Although some heavy-atom-transfer bimolecular reactions can also proceed with important tunneling effects,[53,68] the very dramatic tunneling effects and the leveling off of the rate constants as seen in the current study would be unlikely to occur in bimolecular reactions such as $O + O_2 \rightarrow O_3$ or $O + CO \rightarrow CO_2$[68] at or above ∼150 K for the following reasons. First, the reaction path on the reactant side is not finite, and thus the barrier width would usually be much larger than a unimolecular reaction. Second, the available energy levels for tunneling are not quantized (due to the continuous distribution of the relative translational energies between the two reactants), and the leveling off of the rate constant would be much less dramatic except at extremely low temperature.

SUMMARY

We have calculated the thermal rate constants of the isomerization reaction from the cyclic ozone to the open (normal) form of ozone using dual-level VTST/MT theory. The results showed that the tunneling effects totally dominate the reaction at low temperature, and very significant tunneling effects exist even at 500 K. This is quite unexpected for the motions of oxygen atoms, which are considerably more massive than hydrogen atoms. Even though there is a large energy barrier of ∼25 kcal/mol, the isomerization reactions were predicted to proceed very fast due to the strong tunneling effects and the potential energy surface

crossing of the $1A_1$ and $1A_2$ states. The half-life of the cyclic ozone was predicted as only ~10 s at 200 K and ~70 s at and below 100 K. The reaction also showed significant kinetic isotope effects, especially for the double and triple substitutions (KIE2 and KIE3) with the ^{18}O isotope. Tunneling effects were found to contribute significantly to the kinetic isotope effects. The quantized reactant state tunneling calculation predicted that both the rate constants and the kinetic isotope effects would reach the asymptotic values below ~150 K. Because of the large KIE3 (~10, and thus 10 times longer lifetime), the experimental identification of the cyclic 18_{O_3} might be more promising.

■ ASSOCIATED CONTENT

Supporting Information. Tables of calculated geometries, energies, vibrational frequencies, rate constants, kinetic isotope effects, energy levels, method description, additional references, and sample input files for dynamics calculation. This material is available free of charge via the Internet at http://pubs.acs.org.

■ AUTHOR INFORMATION

Corresponding Author
chewph@ccu.edu.tw

■ ACKNOWLEDGMENT

We are very grateful for the helpful discussion with Prof. Yuan T. Lee, Prof. Chi-Kung Ni, and Prof. Jim J.-M. Lin of the Institute of Atomic and Molecular Sciences, Academia Sinica. This work is supported by the National Science Council of Taiwan, grant number NSC-97-2113-M-194-004. We are grateful to the National Center for High-Performance Computing (NCHC) for providing part of the computing resources.

■ REFERENCES

(1) Crutzen, P. J. *Q. J. R. Meteorol. Soc.* **1970**, *96*, 320.
(2) Stolarski, R. S.; Cicerone, R. J. *Can. J. Chem.* **1974**, *52*, 1610.
(3) Molina, M. J.; Rowland, F. S. *Nature* **1974**, *249*, 810.
(4) Fishman, J.; Crutzen, P. J. *Nature* **1978**, *274*, 855.
(5) Kohlmiller, C. K.; Andrews, L. *J. Am. Chem. Soc.* **1981**, *103*, 2578.
(6) Atkinson, R.; Carter, W. P. L. *Chem. Rev.* **1984**, *84*, 437.
(7) Farman, J. C.; Gardiner, B. G.; Shanklin, J. D. *Nature* **1985**, *315*, 207.
(8) Solomon, S.; Garcia, R. R.; Rowland, F. S.; Wuebbles, D. J. *Nature* **1986**, *321*, 755.
(9) McElroy, M. B.; Salawitch, R. J.; Wofsy, S. C.; Logan, J. A. *Nature* **1986**, *321*, 759.
(10) Crutzen, P. J.; Arnold, F. *Nature* **1986**, *324*, 651.
(11) Barrle, L. A.; Bottenheim, J. W.; Schnell, R. C.; Crutzen, P. J.; Rasmussen, R. A. *Nature* **1988**, *334*, 138.
(12) Lelieveld, J.; Crutzen, P. J. *Nature* **1990**, *343*, 227.
(13) McGrath, M. P.; Clemitshaw, K. C.; Rowland, F. S.; Hehre, W. J. *J. Phys. Chem.* **1990**, *94*, 6126.
(14) Wayne, R. P.; Poulet, G.; Biggs, P.; Burrows, J. P.; Cox, R. A.; Crutzen, P. J.; Hayman, G. D.; Jenkin, M. E.; Le Bras, G.; Moortgat, G. K.; Platt, U.; Schindler, R. N. *Atmos. Environ.* **1995**, *29*, 2677.
(15) Zhang, J.; Lee, Y.-T. *J. Phys. Chem. A* **1997**, *101*, 6485.
(16) (a) Brown, T. L.; LeMay, H. E., Jr.; Bursten, B. E.; Murphy, C. J. *Chemistry*, 10th ed.; Pearson Prentice Hall: New York, 2006; pp 781−782. (b) Wayne, R. P. *Chemistry of Atmospheres*, 2nd ed.; Oxford: New York, 1991; pp 252−263.
(17) (a) El-Awa, A.; Noshi, M. N.; du Jourdin, X. M.; Fuchs, P. L. *Chem. Rev.* **2009**, *109*, 2315. (b) Horie, O.; Moortgat, G. K. *Acc. Chem. Res.* **1998**, *31*, 387.
(18) (a) Laidig, W. D.; Schaefer, H. F. *J. Chem. Phys.* **1981**, *74*, 3411. (b) Borowski, P.; Andersson, K.; Malmqvist, P. Å.; Roos, B. O. *J. Chem. Phys.* **1992**, *97*, 5568. (c) Leininger, M. L.; Schaefer, H. F. *J. Chem. Phys.* **1997**, *107*, 9059. (d) Li, X.; Paldus, J. *J. Chem. Phys.* **1999**, *110*, 2844. (e) Ljubic, I.; Sabljic, A. *J. Phys. Chem. A* **2002**, *106*, 4745. (f) Zhao, Y.; Tishchenko, O.; Gour, J. R.; Li, W.; Lutz, J. J.; Piecuch, P.; Truhlar, D. G. *J. Phys. Chem. A* **2009**, *113*, 5786.
(19) Xantheas, S. S.; Atchity, G. J.; Elbert, S. T.; Ruedenberg, K. *J. Chem. Phys.* **1991**, *94*, 8054.
(20) Ivanic, J.; Atchity, G. J.; Ruedenberg, K. *J. Chem. Phys.* **1997**, *107*, 4307.
(21) Siebert, R.; Schinke, R.; Bittererová, M. *Phys. Chem. Chem. Phys.* **2001**, *3*, 1795.
(22) Siebert, R.; Fleurat-Lessard, P.; Schinke, R; Bittererová, M.; Farantos, S. C. *J. Chem. Phys.* **2002**, *116*, 9749.
(23) Qu, Z.-W.; Zhu, H.; Schinke, R. *J. Chem. Phys.* **2005**, *123*, 204324.
(24) De Vico, L.; Pegado, L.; Heimdal, J.; Söderhjelm, P.; Roos, B. O. *Chem. Phys. Lett.* **2008**, *461*, 136.
(25) Flemmig, B.; Wolczanski, P. T.; Hoffmann, R. *J. Am. Chem. Soc.* **2005**, *127*, 1278.
(26) (a) Truhlar, D. G.; Garrett, B. C. *Acc. Chem. Res.* **1980**, *13*, 440. (b) Truhlar, D. G.; Isaacson, A. D.; Garrett, B. C. In *Theory of Chemical Reaction Dynamics*; Baer, M., Ed.; CRC Press: Boca Raton, FL, 1985; Vol. 4, p 65.
(27) Liu, Y.-P.; Lu, D.-H.; Gonzalez-Lafont, A.; Truhlar, D. G.; Garrett, B. C. *J. Am. Chem. Soc.* **1993**, *115*, 7806.
(28) (a) Liu, Y.-P.; Lynch, G. C.; Truong, T. N.; Lu, D.-H.; Truhlar, D. G.; Garrett, B. C. *J. Am. Chem. Soc.* **1993**, *115*, 2408. (b) Lu, D.-H.; Truong, T. N.; Melissas, V. S.; Lynch, G. C.; Liu, Y.-P.; Garrett, B. C.; Steckler, R.; Isaacson, A. D.; Rai, S. N.; Hancock, G. C.; Lauderdale, J. G.; Joseph, T.; Truhlar, D. G. *Comput. Phys. Commun.* **1992**, *71*, 235.
(29) Truong, T. N.; Lu, D.-H.; Lynch, G. C.; Liu, Y.-P.; Melissas, V. S.; Gonzalez-Lafont, A.; Rai, S. N.; Steckler, R.; Garrett, B. C.; Joseph, T.; Truhlar, D. G. *Comput. Phys. Commun.* **1993**, *75*, 143.
(30) Hu, W.-P.; Liu, Y.-P.; Truhlar, D. G. *J. Chem. Soc., Faraday Trans.* **1994**, *90*, 1715.
(31) Lee, C.; Yang, W.; Parr, R. G. *Phys. Rev. B* **1988**, *37*, 785.
(32) Stephens, P. J.; Devlin, F. J.; Chabalowski, C. F.; Frisch, M. J. *J. Phys. Chem.* **1994**, *98*, 11623.
(33) (a) Dunning, T. H., Jr. *J. Chem. Phys.* **1989**, *90*, 1007. (b) Kendall, R. A.; Dunning, T. H., Jr.; Harrison, R. J. *J. Chem. Phys.* **1992**, *96*, 6796. (c) Woon, D. E.; Dunning, T. H., Jr. *J. Chem. Phys.* **1993**, *98*, 1358.
(34) Page, M.; McIver, J. W., Jr. *J. Chem. Phys.* **1988**, *88*, 922.
(35) Page, M.; Doubleday, C.; McIver, J. W., Jr. *J. Chem. Phys.* **1990**, *93*, 5634.
(36) Møller, C.; Plesset, M. S. *Phys. Rev.* **1934**, *46*, 618.
(37) Knowles, P. J.; Werner, H.-J. *Chem. Phys. Lett.* **1988**, *145*, 514.
(38) Pople, J. A.; Head-Gordon, M.; Raghavachari, K. *J. Chem. Phys.* **1987**, *87*, 5968.
(39) Werner, H.-J.; Knowles, P. J. *J. Chem. Phys.* **1988**, *89*, 5803.
(40) Langhoff, S. R.; Davidson, E. R. *Int. J. Quantum Chem.* **1974**, *8*, 61.
(41) Huang, C.-H.; You, R.-M.; Lian, P.-Y.; Hu, W.-P. *J. Phys. Chem. A* **2000**, *104*, 7200.
(42) Wonchoba, S. E.; Hu, W.-P.; Truhlar, D. G. In *Theoretical and Computational Approaches to Interface Phenomena*; Sellers, H. L.,Golab, J. T., Eds.; Plenum Press: New York, 1994; p 1.
(43) Wonchoba, S. E.; Hu, W.-P.; Truhlar, D. G. *Phys. Rev. B* **1995**, *51*, 9985.
(44) Frisch, M. J.; et al. *Gaussian 03*, revision E.01; Gaussian, Inc.: Wallingford, CT, 2004.
(45) MOLPRO, version 2009.1, designed by H.-J. Werner and P. J. Knowles, 2009.

(46) Corchado, J. C.; Chunag, Y.-Y.; Coitino, E. L.; Truhlar, D. G. *Gaussrate*, version 8.2; University of Minnesota: Minneapolis, MN, 1999.
(47) Chuang, Y.-Y.; et al. *Polyrate-version 8.2*; University of Minnesota: Minneapolis, MN, 1999.
(48) Tyterev, V. G.; Tashkun, S.; Jensen, P.; Barbe, A.; Cours, T. *J. Mol. Spectrosc.* **1999**, *198*, 57.
(49) (a) Shelton, G. R.; Hrovat, D. A.; Borden, W. T. *J. Am. Chem. Soc.* **2007**, *129*, 164. (b) Wu, A.; Mader, A.; Datta, A.; Hrovat, D. A.; Borden, W. T.; Mayer, J. M. *J. Am. Chem. Soc.* **2009**, *131*, 11985.
(50) (a) Ellingson, B. A.; Pu, J.; Lin, H.; Zhao, Y.; Truhlar, D. G. *J. Phys. Chem. A* **2007**, *111*, 10706. (b) Ellingson, B. A.; Truhlar, D. G. *J. Am. Chem. Soc.* **2007**, *129*, 12765. (c) Ellingson, B. A.; Theis, D. P.; Tishchenko, O.; Zheng, J.; Truhlar, D. G. *J. Phys. Chem. A* **2007**, *111*, 13554. (d) Zheng, J.; Truhlar, D. G. *J. Phys. Chem. A* **2009**, *113*, 11919.
(51) (a) Wu, Y.-R.; Hu, W.-P. *J. Am. Chem. Soc.* **1999**, *121*, 10168. (b) Chen, Y.-L.; Hu, W.-P. *J. Phys. Chem. A* **2004**, *108*, 4449.
(52) (a) Albu, T. V.; Lynch, B. J.; Truhlar, D. G.; Goren, A. C.; Hrovat, D. A.; Borden, W. T.; Moss, R. A. *J. Phys. Chem. A* **2002**, *106*, 5323. (b) Zuev, P. S.; Sheridan, R. S.; Albu, T. V.; Truhlar, D. G.; Hrovat, D. A.; Borden, W. T. *Science* **2003**, *299*, 867. (c) Datta, A.; Hrovat, D. A.; Borden, W. T. *J. Am. Chem. Soc.* **2008**, *130*, 6684. (d) Gonzalez-James, O. M.; Zhang, X.; Datta, A.; Hrovat, D. A.; Borden, W. T.; Singleton, D. A. *J. Am. Chem. Soc.* **2010**, *132*, 12548.
(53) (a) Huang, C.-H.; Tsai, L.-C.; Hu, W.-P. *J. Phys. Chem. A* **2001**, *105*, 9945. (b) Fu, Y.-S.; Tsai, S.-C.; Huang, C. H.; Yen, S.-Y.; Hu, W. P.; Yu, S. J. *J. Org. Chem.* **2003**, *68*, 3068.
(54) Khriachtchev, L.; Pettersson, M.; Runeberg, N.; Lundell, J.; Räsänen, M. *Nature (London)* **2000**, *406*, 874.
(55) Khriachtchev, L.; Domanskaya, A.; Lundell, J.; Akimov, A.; Räsänen, M.; Misochko, E. *J. Phys. Chem. A* **2010**, *114*, 4181.
(56) Samartzis, P. C.; Wodtke, A. M. *Phys. Chem. Chem. Phys.* **2007**, *9*, 3054.
(57) Herrebout, W. A.; Delanoye, S. N.; Maes, B. U. W.; van der Veken, B. J. *J. Phys. Chem. A* **2006**, *110*, 13759.
(58) Schlag, E. M.; Rabinovitch, B. S. *J. Am. Chem. Soc.* **1960**, *82*, 5996.
(59) Dubnikova, F.; Lifshitz, A. *J. Phys. Chem. A* **1998**, *102*, 3299.
(60) Goodrow, A.; Bell, A. T.; Head-Gordon, M. *J. Chem. Phys.* **2009**, *130*, 244108.
(61) Waage, E. V.; Rabinovitch, B. S. *J. Phys. Chem.* **1972**, *76*, 1695.
(62) Mueller, K. H.; Walters, W. D. *J. Am. Chem. Soc.* **1951**, *73*, 1458.
(63) (a) Nguyen, T. L.; Vereecken, L.; Hou, X. J.; Nguyen, M. T.; Peeters, J. *J. Phys. Chem. A* **2005**, *109*, 7489. (b) Joshi, A.; You, X.; Barckholtz, T. A.; Wang, H. *J. Phys. Chem. A* **2005**, *109*, 8016.
(64) Cremer, D.; Kraka, E.; Szalay, P. G. *Chem. Phys. Lett.* **1998**, *292*, 97.
(65) Chen, B.-Z.; Anglada, J. M.; Huang, M.-B.; Kong, F. *J. Phys. Chem. A* **2002**, *106*, 1877.
(66) Zhang, P.; Morokuma, K.; Wodtke, A. M. *J. Chem. Phys.* **2005**, *122*, 014106.
(67) Larson, C.; Ji, Y.; Samartzis, P. C.; Quinto-Hernandez, A.; Lin, J. J.; Ching, T.-T.; Chaudhuri, C.; Lee, S.-H.; Wodtke, A. M. *J. Phys. Chem. A* **2008**, *112*, 1105.
(68) Goumans, T. P. M.; Andersson, S. *Mon. Not. R. Astron. Soc.* **2010**, *406*, 2213.